


ORIGINAL ARTICLE

Open Access



Tracked Foley catheter for motion compensation during fusion image-guided prostate procedures: a phantom study

Graham R. Hale^{1,2†}, Filippo Pesapane^{1,3*†} , Sheng Xu¹, Ivane Bakhutashvili¹, Neil Glossop⁴, Baris Turkbey⁵, Peter A. Pinto² and Bradford J. Wood^{1,2}

Abstract

Background: Uncorrected patient or prostate motion may impair targeting prostate areas during fusion image-guided procedures. We evaluated if a prototype “tracked Foley catheter” (TFC) could maintain fusion image alignment after simulated organ motion.

Methods: A pelvic phantom model underwent magnetic resonance imaging (MRI), and the prostate was segmented. The TFC was placed in the phantom. MRI/ultrasound (US) fusion was performed. Four trials were performed varying motion and TFC presence/absence: (1) TFC/no-motion, (2) TFC/motion, (3) no-TFC/no-motion, and (4) no-TFC/motion. To quantify image alignment, screen captures generated Dice similarity coefficient (DSC) and offset distances (ODs) (maximal US-to-MRI distance between edges on fusion images). Three anatomical targets were identified for placement of a needle under fusion guidance. A computed tomography scan was used to measure system error (SE), *i.e.*, the distance from needle tip to intended target.

Results: The TFC presence improved MRI/US alignment by DSC 0.88, 0.88, 0.74, and 0.61 in trials 1, 2, 3, and 4, respectively. Both OD (trial 2 *versus* trial 4, 4.85 ± 1.60 *versus* 25.29 ± 6.50 mm, $p < 0.001$) and SE (trial 2 *versus* trial 4, 6.35 ± 1.31 *versus* 32.16 ± 6.50 mm, $p < 0.005$) were significantly lower when the TFC was present after artificial motion, and significantly smaller OD when static (trial 1 *versus* trial 3, 4.29 ± 1.24 *versus* 6.42 ± 2.29 mm, $p < 0.001$).

Conclusion: TFC provided better image alignment with or without simulated motion. This may overcome system limitations, allowing for more accurate fusion image alignment during fusion-guided biopsy, ablation, or robotic prostatectomy.

Keywords: Focal therapy, Prostatic neoplasms, Image-guided biopsy, Spatial navigation, Surgery (computer-assisted)

Key points

- Outcomes for image-guided prostate biopsy/ablation are dependent upon accurate needle placement.
- Multimodality image fusion allows intra-procedural localisation of tool position and orientation.
- A custom tracked Foley catheter maintained appropriate magnetic resonance imaging/ultrasound-fusion image alignment after movement.
- Tracked Foley catheter may correct intra-procedural prostate motion during fusion-guided prostate procedures.

Background

Within the last decade, fusion image-guided procedures have been applied for the diagnosis and treatment of prostate cancer (PCa). PCa is the most common non-cutaneous cancer in American men: it has been estimated that 164,690 new cases will be diagnosed and that 29,430 American men will die of PCa in 2018 [1].

* Correspondence: pesapane@unimi.it

†Graham R. Hale and Filippo Pesapane contributed equally to this work.

¹Center for Interventional Oncology, Radiology and Imaging Sciences, National Cancer Institute, National Institutes of Health, Bethesda, MD, USA

³Postgraduate School in Radiodiagnostics, Università degli Studi di Milano, Milan, Italy

Full list of author information is available at the end of the article

Recent urologic PCa guidelines have suggested the use of multiparametric MRI (mpMRI) in biopsy naïve men or those with prior negative prostate biopsy [2, 3]. The mpMRI/ultrasound (US) fusion-guided prostate biopsy (FBx) platforms address some of the major limitations of transrectal ultrasound (TRUS)-guided prostate biopsy [4, 5]. Combining the unique capacity to detect clinically significant PCa with the real-time versatility of US [6, 7], FBx increases the accuracy of PCa localisation compared to conventional (blind and random) TRUS biopsies [8, 9], demonstrating higher rates of diagnosis of clinically significant PCa being diagnosed, while simultaneously not detecting indolent PCa that may not require treatment [5, 9, 10]. FBx highlights the benefits that fusion-guided procedures may offer patients; however, challenges and limitations remain. Currently, outcomes for image-guided prostate biopsy and focal ablation are highly dependent upon accurate needle placement at an exact target location [7, 8, 10–14]. Semi-automated computer navigation and guidance allow for the registration (alignment/matching) of pre-procedural imaging (*i.e.*, mpMRI) with real-time intra-procedural imaging (*i.e.*, US). This multimodality image fusion is dependent upon accurate registration of multiple image datasets (mpMRI and US), allowing intra-procedural localisation of the exact position and orientation of tools [15]. Together, registration and fusion enable pre-identified locations to be targeted for biopsy or ablation [16]. After initial MRI/

US image registration and fusion, the US transducer is spatially tracked to provide intra-procedural guidance [7]. However, performance of current FBx platforms and software may markedly degrade during the procedure, due to uncorrected patient or organ motion, or shape deformations. Manual correction of prostate motion and shape deformation can be unreliable due to poor signal-to-noise ratio, out-of-plane prostate motion, and the inability to correct two-dimensional correlations, much less three-dimensional correlations in other planes [16, 17]. Moreover, manual rigid or elastic adjustment of registration may cause offset errors. Likewise, fusion image misalignment may result from intra-procedural repeat registration after organ shift or motion.

A modified Foley catheter with embedded sensors may help correcting for fusion image mismatch, but requires adjustment of the fusion system, methods, and instrumentation (Fig. 1) [18]. With direct real-time feedback of prostate motion (dynamic referencing), this custom tracked Foley catheter (TFC) may provide motion compensation to address the problem of MRI/US misalignment during procedures. This solution uses the same electromagnetic tracking principles as FBx platforms (Fig. 2), and it may improve current system limitations allowing for more accurate image alignment during fusion procedures, such as biopsy, focal PCa ablation, or even possibly fusion-guided robotic prostatectomy in the future, although speculative [15, 19–24]. The present

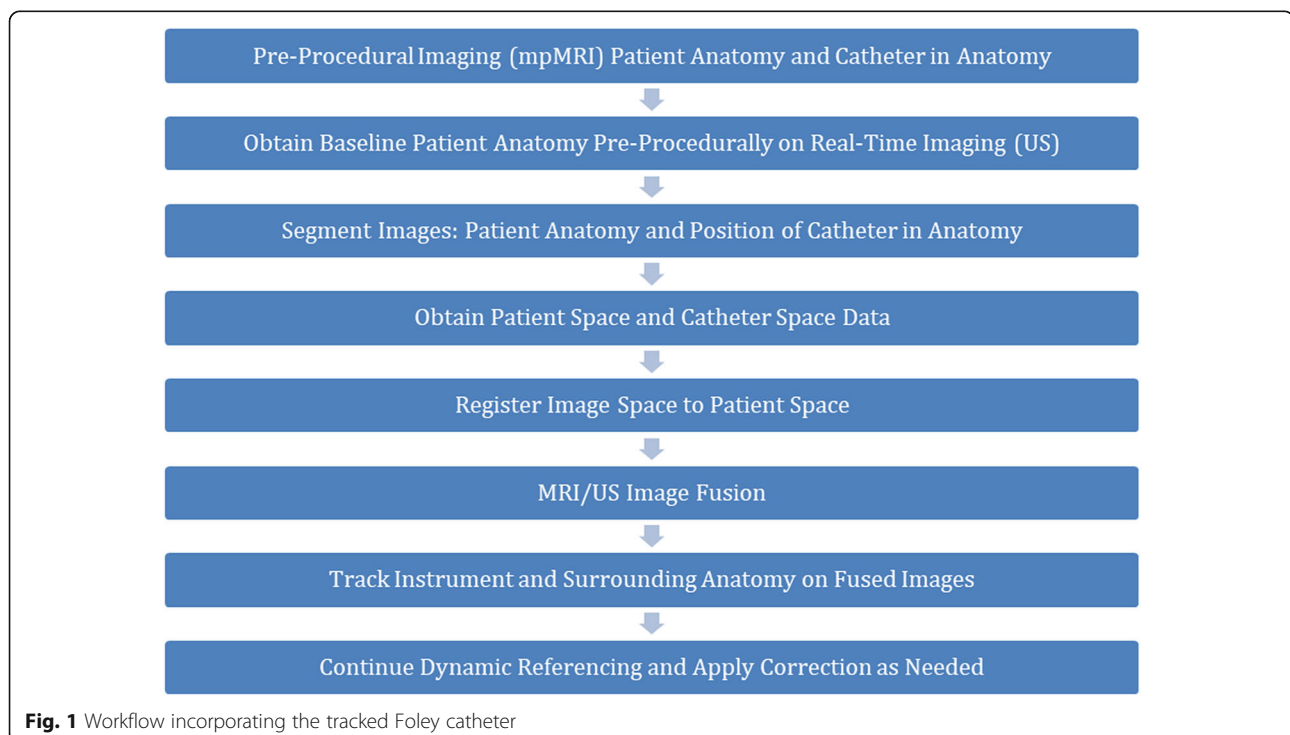


Fig. 1 Workflow incorporating the tracked Foley catheter

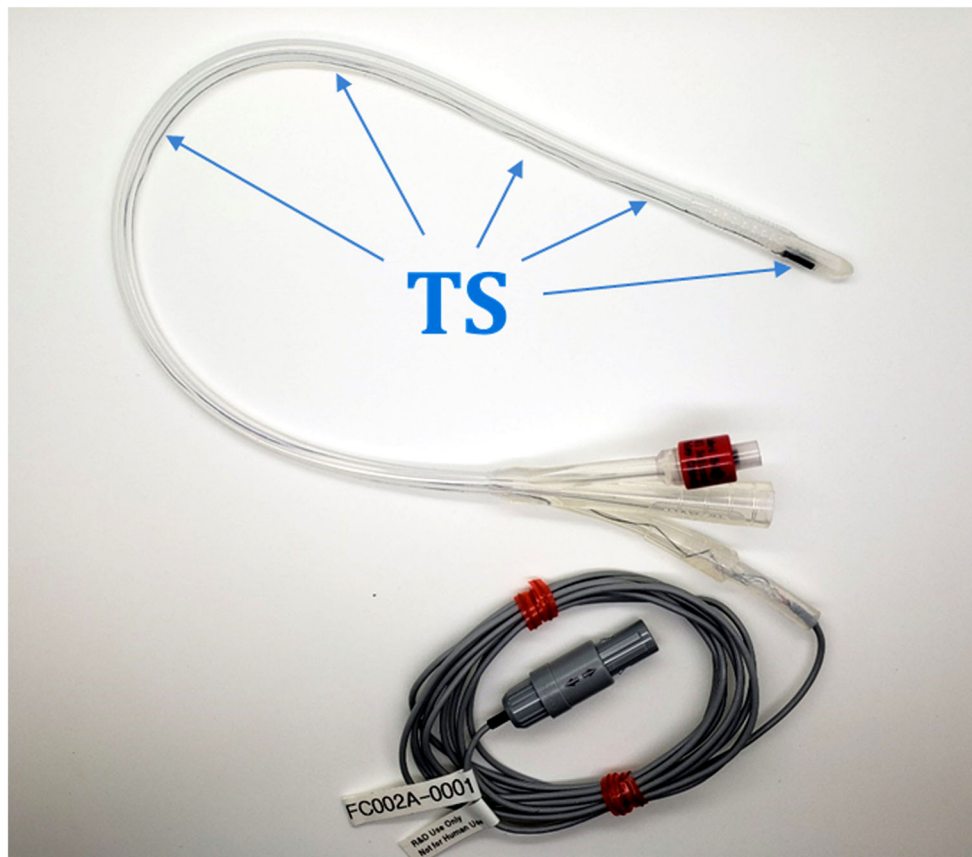


Fig. 2 Tracked Foley catheter (TFC) prototype. The TFC has a six degrees of freedom (forward/backward, up/down, left/right, and rotational movement along x , y , and z axes) tracking sensor (TS) that assumes a complex shape in the urethra and provides real-time tracking data

phantom study aimed to compare fusion image alignment after simulated prostate motion with and without the correction provided by the TFC.

Methods

This study did not involve human subjects or patient data and thus did not require institutional review board approval. Two TFC FBx inexperienced users (one urologist/staff scientist, one research fellow) and one expert fusion software computer science engineer participated in study design and data collection.

This study was performed on one custom pelvic anthropomorphic phantom model (Fig. 3), using the prototype TFC with six degrees of freedom electromagnetic tracking sensors that enable spatial localisation and custom National Institutes of Health fusion software OncoNav (Fig. 4) with an electromagnetic field generator (Uronav, InVivo, Philips Healthcare, Best, Netherlands). The phantom underwent 3-T MRI (Achieva, Philips Healthcare, Best, The Netherlands) with 32-channel cardiac coils, and the prostate capsule was segmented/contoured manually by the expert software engineer, with more than 10 years of experience in prostate capsule

segmentation on MRI and US. The phantom prostate capsule margins were superimposed on axial and sagittal T2-weighted images and transferred to the custom FBx workstation for study trials (Fig. 5).

First, the TFC was placed in the phantom urethra and bladder, and the balloon was inflated with water to secure the TFC in place. Second, an US three-dimensional volume reconstruction of the model prostate was performed after a two-dimensional transrectal US transducer “sweep” (Prostate Triplane 8818, BK Ultrasound, Peabody, USA) from base to apex. Third, the TFC FBx user segmented the phantom prostate edge on triplane US images. Fourth, the MRI volume was registered and fused to the US volume using the custom fusion software. This process was repeated for each trial.

This study consisted of two parts: part A and part B. During part A, the data were collected from intra-experimental screen captures after custom software registration and fusion of MRI/US data, both with and without TFC input. During part B, a copper wire (needle) was placed as closely to prescribed targets as possible, under fusion guidance. The motion induced during part A was both rotational and translational, while only translational

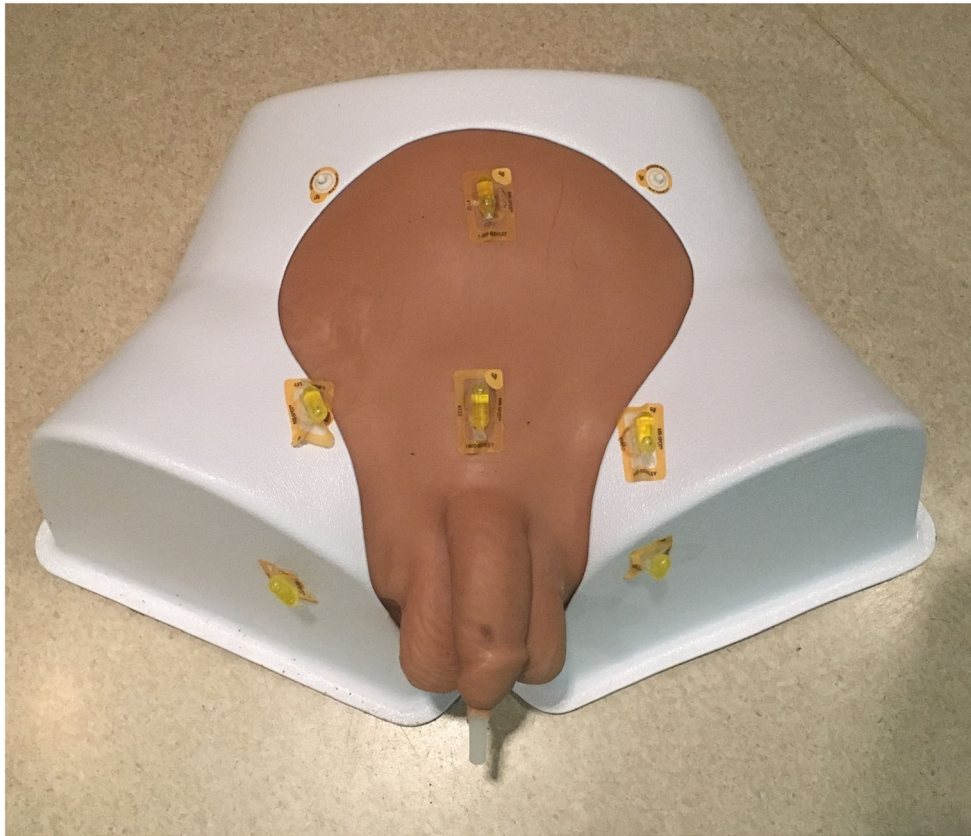


Fig. 3 Custom phantom model. This experiment was performed on a custom pelvic anthropomorphic phantom model. The model contains a catheterisable urethra and urinary bladder, prostate, and surrounding prostatic structures oriented anatomically and visualised on magnetic resonance imaging (MRI), computed tomography (CT), and ultrasound. CT and MRI fiducial markers, which measured simulated motion, are visible on the model surface

motion was induced during part B. Translational motion was created by dropping the computed tomography table, and rotational motion was created by lowering one side of the phantom. Six fiducial marker locations (placed on phantom surface, visible on computed tomography scans) were documented before and after combined motion. Fiducial markers were displaced by the “motion” an average of 12.11 mm with translation and 8° from the horizontal with rotational motion.

During part A, four trial scenarios were created which varied the artificial motion and the presence and absence of TFC input. Screen captures were collected after fusion of MRI/US images during each trial: (1) TFC no-motion, (2) TFC with motion, (3) no-TFC no-motion, and (4) no-TFC with motion. Trials involving no motion were performed first, followed by trials involving motion. Next, Dice similarity coefficients (DSCs) were calculated from screen captures viewed on a picture archiving and communication system in which the prostate edge was best seen on both US and MRI (two per trial: one axial and one sagittal view). Average maximum offset distances (ODs) were calculated from all screen captures

(Fig. 6) across the four scenarios. OD was defined as the distance between the phantom edge on US and perpendicular line striking the same location as seen on the contoured edge on MRI (Fig. 7).

Part B began with the phantom positioned neutrally, repeating the US sweep to build the three-dimensional volume, volume reconstruction, prostate edge segmentation on US, and finally MRI/US fusion using the custom fusion software. Three targets were identified (beginning and end of the neurovascular bundles seen on CT and US), overlaid with a virtual marker that was then targeted with a needle during the same four trials scenarios (trials 1 to 4, above). Artificial motion was induced by dropping the computed tomography table 15 mm for trials 2 and 4. For part B, only translational motion was induced, without rotational motion. After a needle was placed in each target location, assisted by the custom fusion software, system error (SE) was calculated from computed tomography (Brilliance 16, Achieva, Philips Healthcare, Best, The Netherlands). SE was defined as the distance from the tip of the needle to the location of the intended target (neurovascular bundles).

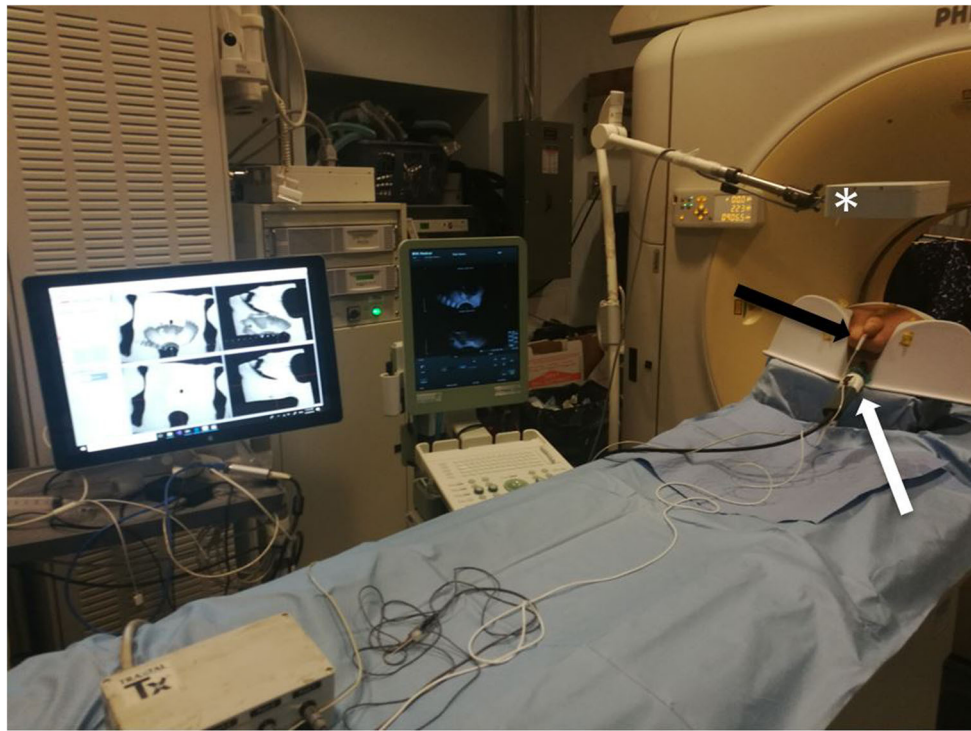


Fig. 4 Tracked Foley catheter (TFC) test-bed experiment. The screen on the left shows the custom fusion biopsy software platform (Onconav, National Institutes of Health, USA). The TFC prototype (*black arrow*) enters the anthropomorphic phantom urethra. Ultrasound transducer in phantom rectum (*white arrow*). Electromagnetic field generator (*asterisk*)

Data were checked for normal or near-normal *versus* non-normal distribution using the Shapiro-Wilk test at 0.05 significance and reported as mean \pm standard deviation. ODs were compared using a *t* test at a significance level of 0.05. Prostate contour two-dimensional area measurements were made on screenshots on MRI, US, and then the area of MRI; US overlap in pixels was used to calculate DSC for each trial. SE distances were compared using a *t* test at a significance level of 0.05. StataSE 15 software was used (StataCorp, College Station, USA).

Results

During part A, 40 total screen captures ($n = 80$ total OD measurements) were saved to compare the 4 trials (10 for each of the 4 trials). OD was significantly lower when the TFC was present *versus* absent both with motion (trial 2 *versus* trial 4, 4.85 ± 1.60 *versus* 25.29 ± 6.50 mm, $p < 0.001$) and without motion (trial 1 *versus* trial 3, 4.29 ± 1.24 *versus* 6.42 ± 2.29 mm, $p < 0.001$). There was no significant difference in OD before and after motion when the TFC data was present (trial 1 *versus* trial 2, 4.29 ± 1.24 *versus* 4.85 ± 1.60 mm, $p = 0.234$). When the TFC was absent, there was significantly higher OD after artificial motion (trial 3 *versus* trial 4, 6.42 ± 2.29 *versus* 25.29 ± 6.50 mm, $p < 0.001$). The mean DSC for trials 1, 2, 3, and 4 was 0.88, 0.88, 0.74, and 0.61, respectively, for

the 8 screen captures in part A. Results concerning the study part A are summarised in Fig. 8.

During part B, 12 computed tomography scans were performed ($n = 12$ total SE measurements) to compare between the 4 trials. SE was significantly smaller when the TFC was present *versus* absent with motion (trial 2 *versus* trial 4, 6.35 ± 1.31 *versus* 32.16 ± 6.50 mm, $p < 0.005$). There was no significant difference in SE before and after motion when the TFC was present (trial 1 *versus* trial 2; 5.57 ± 1.50 *versus* 6.35 ± 1.31 mm, $p = 0.569$). When the TFC was absent, there was significantly higher SE after artificial motion (trial 3 *versus* trial 4, 8.63 ± 4.03 *versus* 32.16 ± 6.50 mm, $p < 0.010$). There was no significant difference in SE when the TFC was present *versus* absent and remained static (trial 1 *versus* trial 3, 5.57 ± 1.50 *versus* 8.63 ± 4.03 mm, $p = 0.284$). Results concerning the study part B are summarised in Fig. 9.

Discussion

This study demonstrated that the TFC can provide active intra-procedural fusion image correction automatically after simulated motion in a model pelvis. Inaccuracies in targeting pre-identified prostate locations are often multifactorial, and may be related to prostate motion or deformation, patient movement, or imaging challenges, including impaired segmentation, image registration or

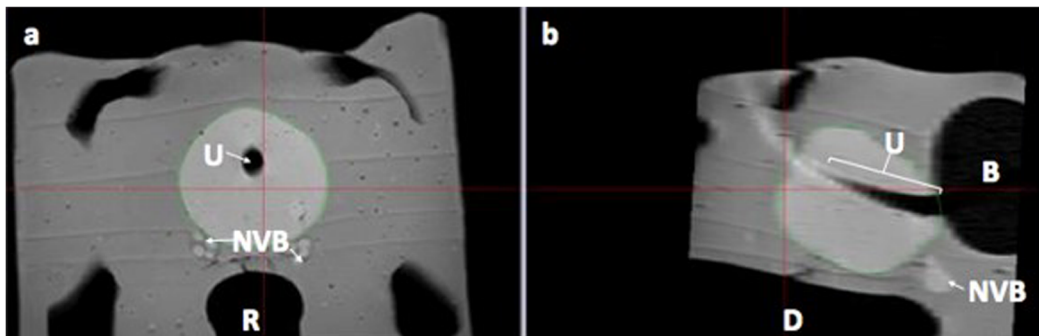


Fig. 5 Contoured prostate capsule. **a** Axial and **(b)** sagittal T2-weighted magnetic resonance images. Note the pelvic phantom model urethra (U), rectum (R), bladder (B), and neurovascular bundles (NVB)

mismatch, and offset of imaging planes [7, 25]. The TRUS plane for acquisition, registration, and manual intra-procedural alignment correction is slightly offset from that of the MRI, adding to the challenge [26]. Current FBx platforms and software systems inadequately compensate for motion of the prostate, thus limiting the accuracy of this technology, even when the prostate is mostly stationary and static. Additionally, registration methods and techniques are widely variable and non-standardised across many commercial platforms, contributing toward variable outcomes from those centres performing or

reporting image-guided prostate procedures [27]. Standardisation of rigid and elastic registration combined with dynamic referencing of the prostate might reduce the operator variability and the inaccuracies induced by subjectivity, experience, and variable intra-procedural corrections of misaligned fusion images.

Within the TFC, six degrees of freedom tracking sensors induce a weak current in the presence of a rapidly changing magnetic field, enabling spatial localisation on imaging (same principle of electromagnetic tracking in existing FBx systems) [18, 28]. The TFC resides within

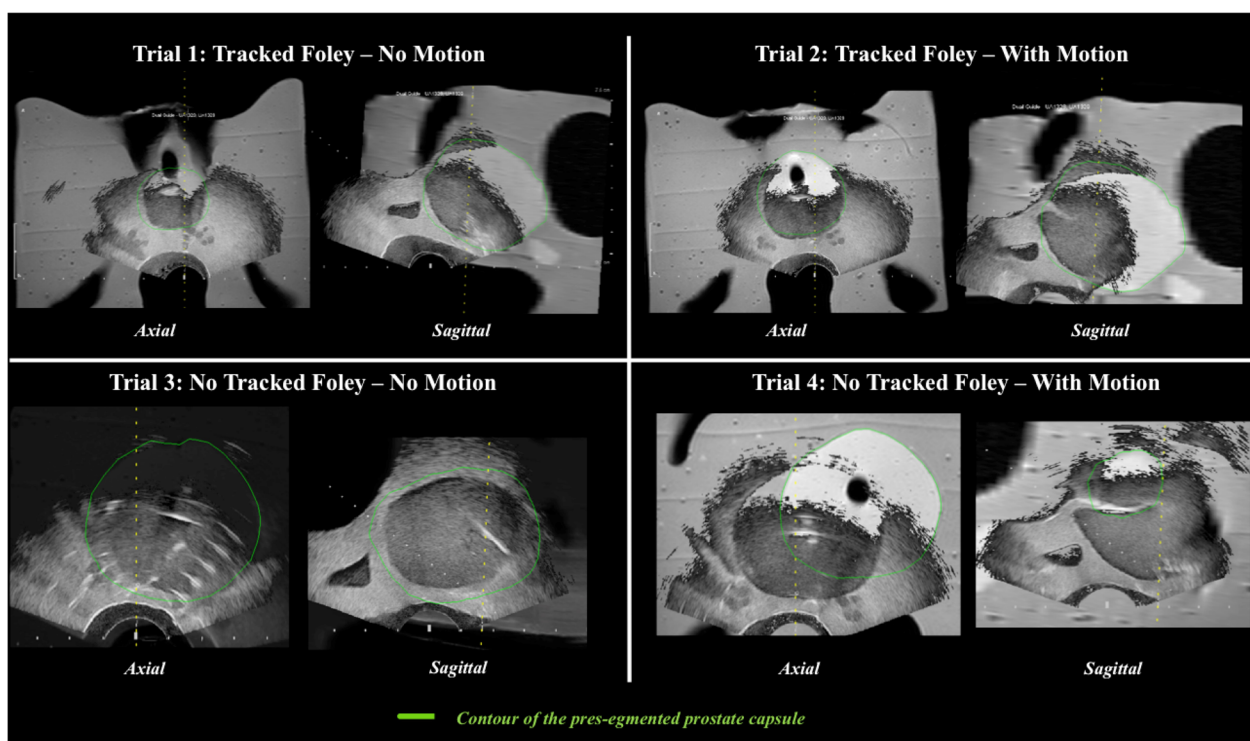


Fig. 6 Intra-experimental screen captures from trials 1 to 4: magnetic resonance imaging (MRI)/ultrasound (US) fusion images, displayed with variable windowing blending MRI and US. Note trial 3 images showing the US predominantly on the left and more MRI on the right. The green contour is the pre-segmented prostate capsule from the pre-procedural MRI

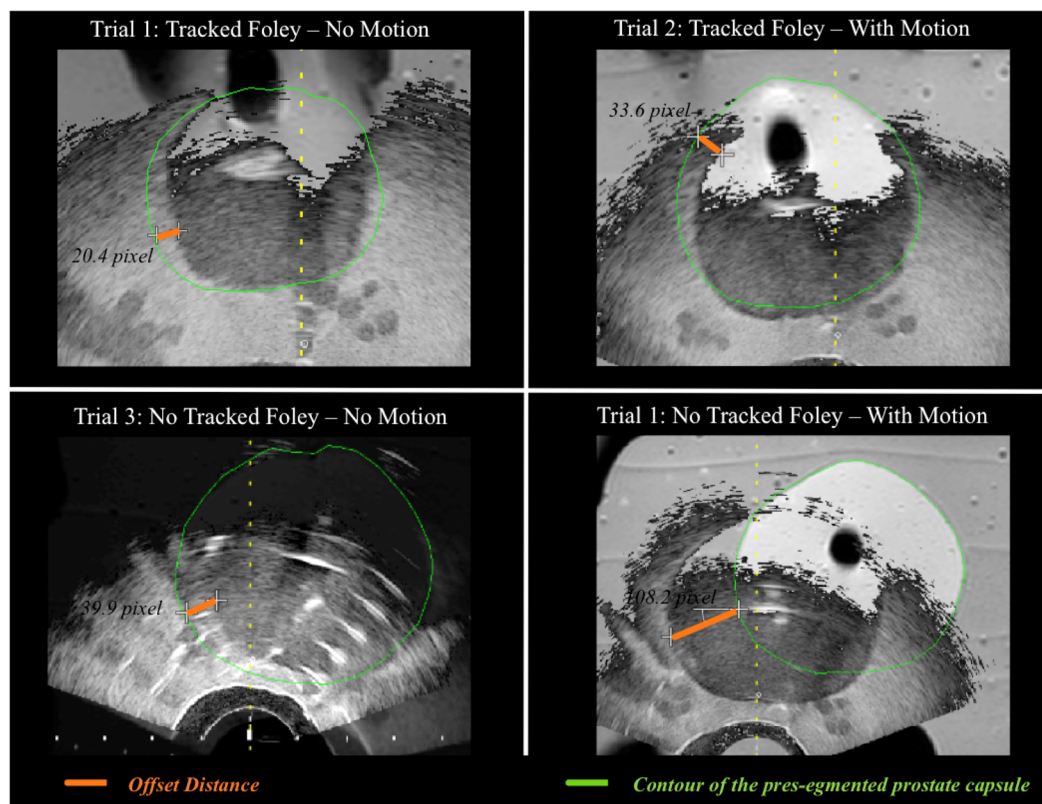


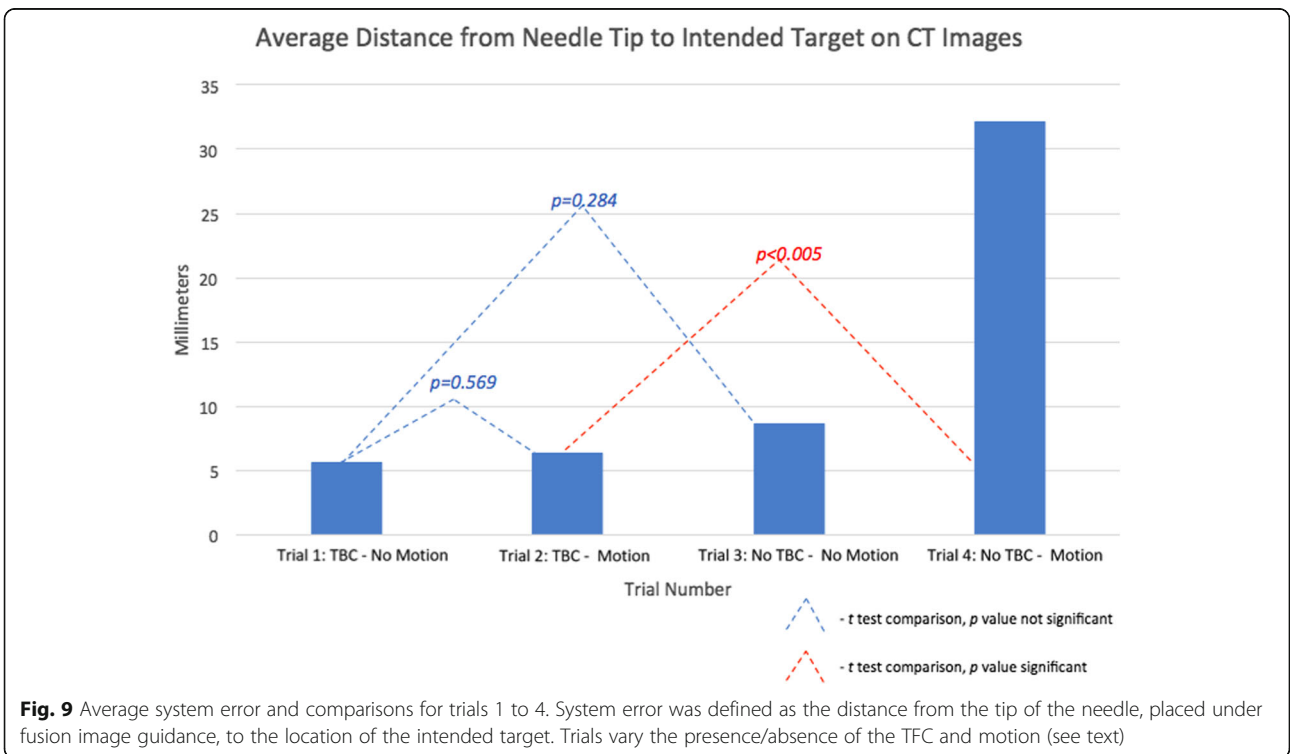
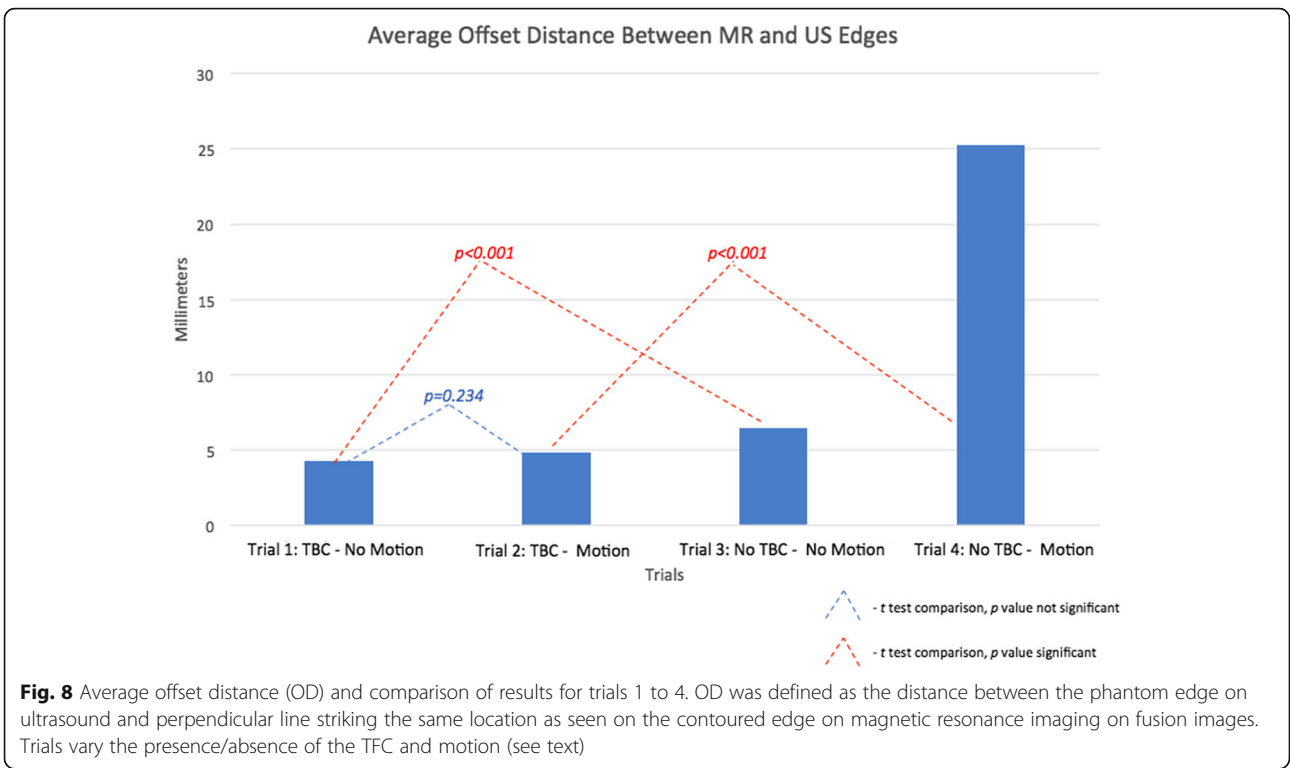
Fig. 7 Maximum offset distance (OD) between the phantom edge on ultrasound (US) and magnetic resonance imaging (MRI) on the axial plane. OD was defined as the distance between the phantom edge on US and perpendicular line striking the same location as seen on the contoured edge on MRI. The green contour is the pre-segmented prostate capsule from the pre-procedural MRI

the urethra, a non-linear central pathway. This urethral path is less altered by prostate motion (especially rotational) or deformation, than other areas of the prostate, and can act as a standardisation tool or “home reference” for correcting fusion image mismatch during a procedure or surgery. Although speculative, it is possible that FBx can perhaps then be more accurately performed in the presence of prostate motion, since the motion of the urethra (and TFC within) can provide real-time referencing information, even with poor image visualisation. The fusion image mismatch can thus automatically be accounted for, and a correction may be computed and applied to restore the initial registration in real time.

During image-guided prostate procedures, the patient often moves involuntarily due to pain, discomfort, and/or pressure related to the insertion of needles or TRUS transducer. Moreover, a TRUS transducer can cause distortion of the contour of the prostate during the FBx. Finally, focal blood, local anaesthetic, bowel gas, dissection, bladder filling, or respiratory motion of the patient may cause shifting of the prostate, especially when the patient is in the prone position [18]. The TFC has the ability to maintain appropriate MRI/US fusion image alignment after simulated organ/patient motion in

a catheterisable pelvic phantom model. All three methods of evaluation (DSC, OD, SE) supported the potential benefit of the TFC.

The TFC core concept of active intra-procedural fusion image correction may potentially be applied to other procedures, settings, or organs with additional hardware components and software [18]. The TFC ability to maintain accurate image alignment after motion could not only benefit existing procedures using fusion imaging (FBx, trans-perineal FBx, focal PCa ablations), but also potentially enable fusion guidance within robotic platforms [8, 12, 15, 16, 19–24, 29–31]. In addition to aid in alignment after simulated prostate motion, this study also indicated that the TFC may aid in more accurate image alignment while the patient remains static. It is possible this finding may stem from the fact that there is some degree of organ motion or deformation when the US transducer is introduced in the rectum, either during the initial US sweep or at any other point during image-guided procedures. The adjustments provided by the TFC may automatically correct for this subtle organ motion or deformation. Our data indicated increased fusion image alignment when the TFC correction was available and no simulated motion was induced,



reporting significantly smaller OD in this scenario. Reported DSC scores showed a similar trend. Although the TFC SE was favoured when compared to no TFC SE when static, the results were not statistically significant.

Standardisation and reproducibility of current image-guided prostate procedures have been less than ideal [5, 9, 10]. Accordingly, there is an urgent need for hardware, systems, and methods for maintaining accurate registration between pre-procedural and intra-procedural images. Image-guided prostate procedures require operator experience for reliable registration of mpMRI/US images and for accurate targeting of pre-identified areas [8, 17, 32]. The TFC may help with the issue of prostate motion by providing a standardised/semi-automated method of maintaining the original registration. Moreover, computer-assisted biopsy systems may facilitate more widespread and standardised use of FBx, even by novice operators who may be uncomfortable manipulating dedicated navigation software [25, 32]. On the other hand, some intrinsic limitations are still present such as the general contraindications for MRI (e.g., the claustrophobia and the presence of a magnetic field or of the pacemakers) and the current failure rate of TRUS-guided biopsy [12, 33–36]. Additional research may explore the extent to which the TFC aids in fusion image alignment when the prostate is static, specifically among novice FBx users.

In our study, fusion image alignment with and without the TFC was compared in three ways with similar results and one method physically targeted region of interests with needles. However, there were several limitations of this study. The physical targeting of identified structures with needles damaged the phantom model somewhat and limited the number of SEs that could be measured on one custom anthropomorphic phantom. There was also no easy and effective way to blind the operator to the presence or absence of the TFC and artificial motion without crippling the study. It remains to be seen whether (and in which scenarios) this solution might prove worthy of the cost and risks associated with an additional catheterisation procedure. Also speculative is the eventual utility for addressing intra-operative prostate organ motion during robotic prostatectomy, which suffers even greater dynamic referencing challenges and shortcomings than FBx. The TFC merits evaluation in a clinical trial setting for biopsy, ablation, and robotic prostatectomy.

In conclusion, fusion-guided prostate procedures have proven benefits. However, fusion biopsy is not yet standardised and suffers from variability and challenges in maintaining accurate image alignment as well as a dearth of tools for facilitated and semi-automated registration. Challenges remain in maintaining registration integrity, procedural standardisation, and reproducibility that may limit the benefits or adoption of fusion guidance. A custom

TFC maintained accurate fusion image alignment after movement and provided significantly better fusion image alignment when static. The inherent challenges of maintaining fusion image alignment may be addressed by this additional smart device, in the presence of an electromagnetic field generator. Although yet to be proven, a TFC may help address clinical needs related to standardisation and correction of intra-procedural prostate motion during fusion-guided prostate procedures such as biopsy, ablation, or robotic prostatectomy.

Abbreviations

DSC: Dice similarity coefficient; FBx: Fusion-guided biopsy; mpMRI: Multiparametric magnetic resonance imaging; MRI: Magnetic resonance imaging; OD: Offset distance; PCa: Prostate cancer; SE: System error; TFC: Tracked Foley catheter; TRUS: Transrectal ultrasound; US: Ultrasound

Acknowledgements

Thank you to those offering research contributions: Stephanie Harmon, Marcin Czarniecki, Samuel A. Gold, Kareem N. Rayn, Jonathan B. Bloom, and Sherif Mehrlivand.

Authors' contributions

SX, NG, PAP, BT, and BJW designed the work. SX created the new software used in the work. GRH and FP analysed and interpreted the data, and they were major contributors in writing the manuscript. SX, GRH, IB, and FP performed the experiment. BT and BJW were major revisors of the manuscript. BJW is the scientific guarantor. All authors read and approved the final manuscript.

Funding

This study was supported by the NIH Center for Interventional Oncology and the Intramural Research Program of the National Institutes of Health (NIH), Z01 grant# 1ZID BC011242 and CL040015. This research was also made possible through the National Institutes of Health (NIH) Medical Research Scholars Program, a public-private partnership supported jointly by the NIH and generous contributions to the Foundation for the NIH from the Doris Duke Charitable Foundation, Genentech, the American Association for Dental Research, the Colgate-Palmolive Company, Elsevier, alumni of student research programs, and other individual supporters via contributions to the Foundation for the National Institutes of Health.

Availability of data and materials

The datasets used and/or analysed during the current study are available from the corresponding author on reasonable request.

Ethics approval and consent to participate

Institutional Review Board approval was not required because the research does not involve human populations or animals.

Consent for publication

Not applicable

Competing interests

NIH and Philips have a Cooperative Research and Development Agreement. NIH has intellectual property in the field patent: "System, methods, and instrumentation for image guided prostate treatment" US Patent number: 8948845, with inventors/authors BW and NG. NIH and Philips (InVivo Inc) have a licensing agreement. NIH and authors receive royalties for a licensing agreement with Philips/InVivo Inc. Author NG is employed by Arcitrax, Inc., which owns patents and is pursuing active research in the field. NIH does not endorse or recommend any commercial products, processes, or services. The views and opinions of authors expressed on NIH websites do not necessarily state or reflect those of the US Government.

Author details

¹Center for Interventional Oncology, Radiology and Imaging Sciences, National Cancer Institute, National Institutes of Health, Bethesda, MD, USA. ²Urologic Oncology Branch, National Cancer Institute, National Institutes of Health, Bethesda, MD, USA. ³Postgraduate School in Radiodiagnostics, Università degli Studi di Milano, Milan, Italy. ⁴Arcitrix, Toronto, Canada. ⁵Molecular Imaging Program, National Cancer Institute, National Institutes of Health, Bethesda, MD, USA.

Received: 27 August 2019 Accepted: 17 February 2020

Published online: 16 April 2020

References

- American Cancer Society. Key statistics for prostate cancer. Available via <https://www.cancer.org/cancer/prostate-cancer/about/key-statistics.html>. Published 2018. Updated January 4, 2018
- [NG131] Ng. Prostate cancer: diagnosis and management. Available via <https://www.nice.org.uk/guidance/ng131/chapter/Recommendations#assessment-and-diagnosis>. Published 2019
- European Association of Urology. Prostate Cancer. Available via <https://uroweb.org/guideline/prostate-cancer/>. Published 2019
- Turkbey B, Brown AM, Sankineni S, Wood BJ, Pinto PA, Choyke PL (2016) Multiparametric prostate magnetic resonance imaging in the evaluation of prostate cancer. *CA Cancer J Clin* 66:326–336. <https://doi.org/10.3322/caac.21333>
- George AK, Pinto PA, Rais-Bahrami S (2014) Multiparametric MRI in the PSA screening era. *Biomed Res Int* 2014:465816. <https://doi.org/10.1155/2014/465816>
- Ahmed HU, El-Shater Bosaily A, Brown LC et al (2017) Diagnostic accuracy of multi-parametric MRI and TRUS biopsy in prostate cancer (PROMIS): a paired validating confirmatory study. *Lancet*. [https://doi.org/10.1016/S0140-6736\(16\)32401-1](https://doi.org/10.1016/S0140-6736(16)32401-1)
- Xu S, Kruecker J, Turkbey B et al (2008) Real-time MRI-TRUS fusion for guidance of targeted prostate biopsies. *Comput Aided Surg* 13:255–264. <https://doi.org/10.3109/10929080802364645>
- Pinto PA, Chung PH, Rastinehad AR et al (2011) Magnetic resonance imaging/ultrasound fusion guided prostate biopsy improves cancer detection following transrectal ultrasound biopsy and correlates with multiparametric magnetic resonance imaging. *J Urol* 186:1281–1285. <https://doi.org/10.1016/j.juro.2011.05.078>
- Kasivisvanathan V, Rannikko AS, Borghi M et al (2018) MRI-targeted or standard biopsy for prostate-cancer diagnosis. *N Engl J Med*. <https://doi.org/10.1056/NEJMoa1801993>
- Valerio M, Donaldson I, Emberton M et al (2015) Detection of clinically significant prostate cancer using magnetic resonance imaging-ultrasound fusion targeted biopsy: a systematic review. *Eur Urol* 68:8–19. <https://doi.org/10.1016/j.eururo.2014.10.026>
- Comud F, Roumiguie M, Barry de Longchamps N et al (2018) Precision matters in MR imaging-targeted prostate biopsies: evidence from a prospective study of cognitive and elastic fusion registration transrectal biopsies. *Radiology*:162916. <https://doi.org/10.1148/radiol.2017162916>
- Pesapane F, Patella F, Fumarola EM et al (2018) The prostate cancer focal therapy. *Gland Surg* 7:89–102. <https://doi.org/10.21037/gs.2017.11.08>
- Bonekamp D, Jacobs MA, El-Khouli R, Stoianovici D, Macura KJ (2011) Advancements in MR imaging of the prostate: from diagnosis to interventions. *Radiographics* 31:677–703. <https://doi.org/10.1148/rg.313105139>
- Pesapane FSC, De Visschere P, Villeirs G (2019) T-staging of prostate cancer: identification of useful signs to standardize detection of posterolateral extraprostatic extension on prostate MRI. *Clin Imaging* 59:1–7. <https://doi.org/10.1016/j.clinimag.2019.08.007>
- Wood BJ, Kruecker J, Abi-Jaoudeh N et al (2010) Navigation systems for ablation. *J Vasc Interv Radiol* 21:S257–S263. <https://doi.org/10.1016/j.jvir.2010.05.003>
- Venkatesan AM, Wood BJ (2014) Advanced tools and devices: navigation technologies, automation, and robotics in percutaneous interventions. In: Ahrar K, Gupta S (Eds) *Percutaneous image-guided biopsy*, 1st edn. Springer Nature, Heidelberg
- Calio B, Sidana A, Sugano D et al (2017) Changes in prostate cancer detection rate of MRI-TRUS fusion vs systematic biopsy over time: evidence of a learning curve. *Prostate Cancer Prostatic Dis* 20:436–441. <https://doi.org/10.1038/pcan.2017.34>
- Glossop N, Bradford JW (2015) System, methods, and instrumentation for image guided prostate treatment. United States US Patent US8948845B2
- Wood BJ, Locklin JK, Viswanathan A et al (2007) Technologies for guidance of radiofrequency ablation in the multimodality interventional suite of the future. *J Vasc Interv Radiol* 18:9–24. <https://doi.org/10.1016/j.jvir.2006.10.013>
- Phee SJ, Yang K (2010) Interventional navigation systems for treatment of unresectable liver tumor. *Med Biol Eng Comput* 48:103–111. <https://doi.org/10.1007/s11517-009-0568-3>
- Bale R, Widmann G (2007) Navigated CT-guided interventions. *Minim Invasive Ther Allied Technol* 16:196–204. <https://doi.org/10.1080/13645700701520578>
- Valerio M, Cerantola Y, Eggener SE et al (2017) New and established technology in focal ablation of the prostate: a systematic review. *Eur Urol* 71:17–34. <https://doi.org/10.1016/j.eururo.2016.08.044>
- Tay KJ, Schulman AA, Sze C, Tsvivan E, Polascik TJ (2017) New advances in focal therapy for early stage prostate cancer. *Expert Rev Anticancer Ther* 17:737–743. <https://doi.org/10.1080/14737140.2017.1345630>
- Ouzzane A, Btrouni N, Valerio M, Rastinehad A, Colin P, Ploussard G (2017) Focal therapy as primary treatment for localized prostate cancer: definition, needs and future. *Future Oncol* 13:727–741. <https://doi.org/10.2217/fon-2016-0229>
- Xu H, Lasso A, Guion P et al (2013) Accuracy analysis in MRI-guided robotic prostate biopsy. *Int J Comput Assist Radiol Surg* 8:937–944. <https://doi.org/10.1007/s11548-013-0831-9>
- Puech P, Ouzzane A, Gaillard V et al (2014) Multiparametric MRI-targeted TRUS prostate biopsies using visual registration. *Biomed Res Int* 2014:819360. <https://doi.org/10.1155/2014/819360>
- Venderink W, de Rooij M, Sedelaar JPM, Huisman HJ, Futterer JJ (2016) Elastic versus rigid image registration in magnetic resonance imaging-transrectal ultrasound fusion prostate biopsy: a systematic review and meta-analysis. *Eur Urol Focus*. <https://doi.org/10.1016/j.euf.2016.07.003>
- Franz AM, Haidegger T, Birkfellner W, Cleary K, Peters TM, Maier-Hein L (2014) Electromagnetic tracking in medicine—a review of technology, validation, and applications. *IEEE Trans Med Imaging* 33:1702–1725. <https://doi.org/10.1109/TMI.2014.2321777>
- Natarajan S, Jones TA, Priester AM et al (2017) Focal laser ablation of prostate cancer: feasibility of magnetic resonance imaging/ultrasound fusion for guidance. *J Urol*. <https://doi.org/10.1016/j.juro.2017.04.017>
- van den Bos W, Scheltema MJ, Siriwardana AR et al (2017) Focal irreversible electroporation as primary treatment for localized prostate cancer. *BJU Int*. <https://doi.org/10.1111/bju.13983>
- Chaussy CG, Thuroff S (2017) High-intensity focused ultrasound for the treatment of prostate cancer: a review. *J Endourol* 31:S30–S37. <https://doi.org/10.1089/end.2016.0548>
- Puech P, Rouviere O, Renard-Penna R et al (2013) Prostate cancer diagnosis: multiparametric MR-targeted biopsy with cognitive and transrectal US-MR fusion guidance versus systematic biopsy—prospective multicenter study. *Radiology* 268:461–469. <https://doi.org/10.1148/radiol.13121501>
- Feychting M (2005) Health effects of static magnetic fields—a review of the epidemiological evidence. *Prog Biophys Mol Biol* 87:241–246. <https://doi.org/10.1016/j.pbiomolbio.2004.08.007>
- Verma S, Bhavsar AS, Donovan J (2014) MR imaging-guided prostate biopsy techniques. *Magn Reson Imaging Clin N Am* 22:135–144, v. <https://doi.org/10.1016/j.mric.2014.01.002>
- Borghesi M, Ahmed H, Nam R et al (2017) Complications after systematic, random, and image-guided prostate biopsy. *Eur Urol* 71:353–365. <https://doi.org/10.1016/j.eururo.2016.08.004>
- Pesapane F, Czarniecki M, Suter MB, Turkbey B, Villeirs G (2018) Imaging of distant metastases of prostate cancer. *Med Oncol* 35:148. <https://doi.org/10.1007/s12032-018-1208-2>

Publisher's Note

Springer Nature remains neutral with regard to jurisdictional claims in published maps and institutional affiliations.